Preliminary Design and Optimization of a CubeSat Demonstrator for an Origami-inspired Deployable Structure

Velázquez Navarro, Ester ; Solano-López, Pablo ; Uriol Balbin, I.

DOI
10.2514/6.2024-2255

Publication date
2024

Document Version
Final published version

Published in
Proceedings of the AIAA SCITECH 2024 Forum

AIAA SciTech Forum
8-12 January 2024, Orlando, FL
AIAA SCITECH 2024 Forum

10.2514/6.2024-2255

Preliminary Design and Optimization of a CubeSat Demonstrator for an Origami-inspired Deployable Structure

Ester Velázquez Navarro* and Pablo Solano-López.†
Aerospace Systems and Transport Research Group, Universidad Rey Juan Carlos, Fuenlabrada, 28942, Spain

Ines Uriol Balbin‡
Delft University of Technology, Delft, South Holland, 2629 HS, The Netherlands

The demand for pressurized, large structures in space, such as habitats or fuel deposits, is increasing as the space industry grows. The limited payload volume of launch vehicles, combined with their highly constrained shape, presents a significant challenge for these structures. Origami-inspired deployable structures have emerged as a potential solution for this problem. This work aims to design and optimize an origami-inspired deployable structure for use as a technology demonstrator in a 12U CubeSat. The choice of pattern, deployment mechanism, and material considerations are discussed as they are relevant in the initial configuration of the structural prototype. By combining two different types of printable materials, it is possible to create a pattern that is more flexible without the use of mechanical hinges. Then two different modeling methods are analyzed in order to study their physical behavior. Once all the desired configurations are computed, an optimization process is applied in order to obtain the most suitable one under the pre-defined requirements.

Nomenclature

a	=	side length of the base regular polygon
b	=	Kresling triangle hypotenuse
c	=	Kresling triangle leg (which is not a)
h	=	height of flat pattern
h_3	=	height of 3D pattern
$h_{3_{1,2}}$	=	height of the 3D pattern for bi-stable states
n	=	number of sides of the polygon circumscribed
N	=	number of rings of the pattern

I. Introduction

Origami, the ancient art form of paper folding, has transcended its traditional applications to inspire innovative engineering solutions in multiple fields [1]. The inherent adaptability in origami patterns has promising applications in the domain of deployable space structures, where compactness during launch and expansive configurations in orbit are driving requirements [2].

A potential use of the properties of origami lies in large, pressurized structures in space, such as habitats and fuel depots. Such structures could use flexible or deployable engineering solutions because of the limited payload volume

*Laboratory researcher, Aerospace Engineering, ester.velazquez@urjc.es
†Assistant Professor, Aerospace Engineering, pablo.solano@urjc.es
‡Lecturer, Faculty of Aerospace Engineering, i.uriolbalbin@tudelft.nl

that launchers can offer [3]. For instance, Yang et al. [4] carried out a volume optimization for this particular application which highlights the advantages of this approach versus the conventional rigid habitat solution.

However, there are still open questions regarding the material selection and in-orbit performance for this type of application. For this reason, this work aims to advance our understanding of origami-inspired structures by investigating their technical viability through the development of a deployment demonstrator in a 12U CubeSat. CubeSats have served in the past as a convenient platform to demonstrate new technologies, a recent example of this can be found in the LightSail mission which aimed to demonstrate controlled solar sailing in Earth orbit[5].

The proposed design of the CubeSat can be seen in Fig. 1. In the proposed design, a large part of the volume in the satellite is reserved for the demonstrator and the deployment mechanism, reserving the remaining volume for the rest of the CubeSat subsystems.

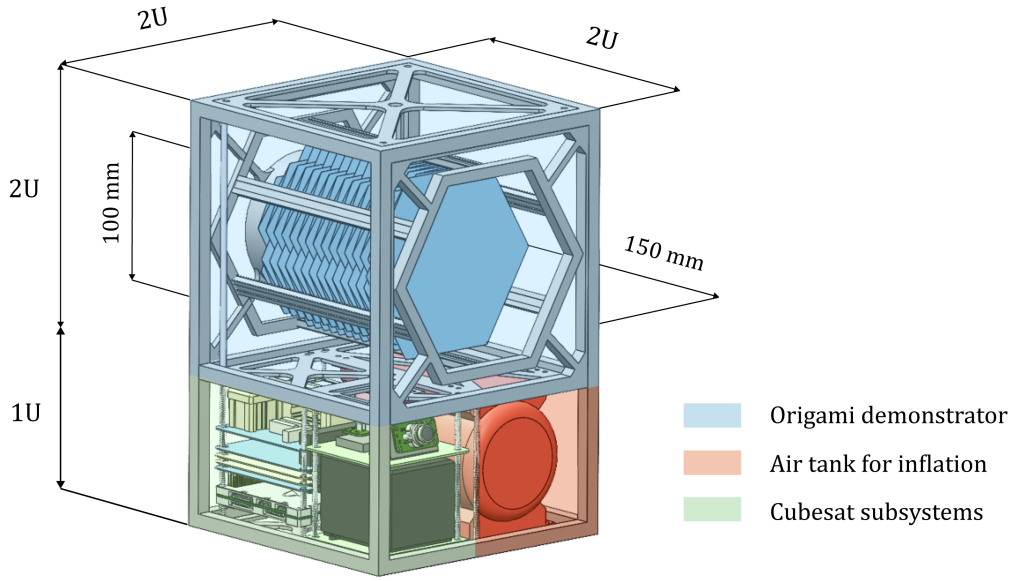

Fig. 1 12U prototype with the origami structure

The work presented here focuses on the design, optimization and numerical modeling of the deployable structure present within the CubeSat. First, a short description of the pattern and the optimization process is included. Then, the different numerical models are described followed up by the obtained results and conclusions.

A. Pattern selection

Since the origami structure is ultimately envisioned as a demonstrator for future human habitats or as fuel tanks it calls for a cylindrical pattern. The most common patterns used for this kind of structures are the Miura-Ori [6], the Yoshimura [7], and the Kresling [8], as presented in Fig. 2.The patterns are shown as unit cell (2D to be assembled) and a 3-dimension (3D) diagram of the deployed origami cylinder. In the 2D diagram, the ridges and valleys foldlines are represented by solid and dashed lines, respectively.

Current state-of-the-art origami-like space structures are based on Miura-ori pattern, becoming the most used one. [1] The reason under this choice is mainly because its high degree of symmetry and its single degree of freedom, also, as it was the first to be implemented, it has more flight hours and so it is considered to be more *robust* from a design point of view. Nevertheless, for the application that is under study in this work, *i.e.*, a cylindrical structure, it has been concluded after several analysis [9] that Kresling and Yoshimura patterns offer a better packaging ratio and some manufacturing advantages.

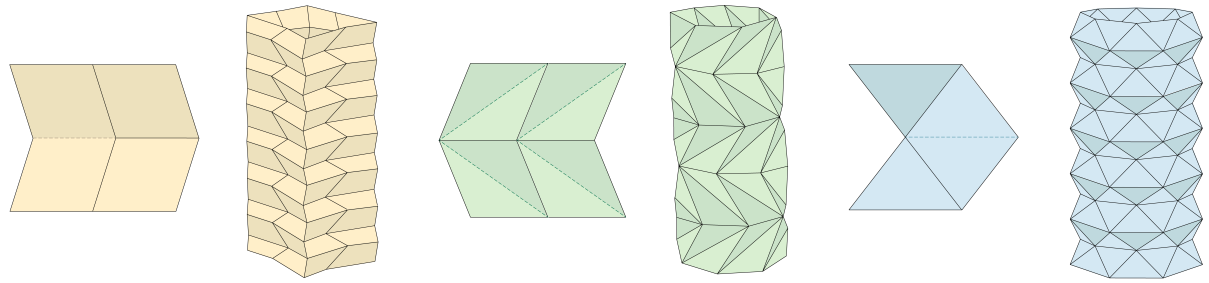

Fig. 2 Origami Patterns in 2D and 3D configurations

As it is defined by Suh et al. [7], a Yoshimura novel pattern allows the structure to be compressed during transportation and then deployed into a very rigid structure. On the other hand, the Kresling pattern, aside of high scalability potential, it also has bistability properties. Among both of them, the selection was based on deployment method during demonstrator flight based on the previous study made by Sachithanandan [10]. A trade-off analysis was made based on the weight, inner volume, scalability and deployment predictability. A high level description of the trade-off can be observed in Table 1. The outcome of this study pointed at the Kresling pattern deployed with inflation being the most favorable pattern in this scenario. Therefore, the Kresling pattern is the one developed and analyzed in this study.

Table 1 Pattern tradeoff. Divided by excellent (green), meet requirements (blue) and average (yellow). [10]

Tradeoff Criteria	Weigth	Inner Volume	Scalability	Deployment Predictability
Yoshimura via Telescopic Deployment				
Kresling Deployment via Inflation				

B. Optimization

Multi-objective optimization for any structure has been intensely studied for the last decade. In the case of origami structures, it is required to highlight the only study with a similar purpose, the one described by Yang et al. [11]. They studied the *"Multi-objective optimization of multi-cell tubes with origami patterns for energy absorption"*, with the aim to find the optimal designs with low initial peak force, high specific energy absorption and small fluctuation of the crushing force. Thus, the method used was the RMS (Response Surface Method) in order to formulate the objective functions. RMS was introduced by Box and Wilson [12] and it is described as a collection of mathematical and statistical techniques in order to analyze problems by an empirical model.

Nevertheless, this study is based on another common way to solve multi-objective optimization by implementing optimization libraries or frameworks. In this case, the method selected was the DAKOTA framework, which offers the algorithms required for performing samplings, meta-model construction and robust genetic optimization algorithms [13].

In this case, the optimization was based on Genetic Algorithms as meta-heuristic strategy with the implementation of surrogate models and the Latin Hypercube sampling (LHS), developed by McKay et al. [14]. Within this DAKOTA tool, selected method has been the MOGA (Multi-objective Genetic Algorithm), *i.e.* a global optimization method which develops a Pareto optimization for multiple objectives.

II. Numerical Model

A. Description

Due to the advantages of the Kresling pattern [8] this study will be based on this pattern, **developing an optimal design for the expected application**. The prototype of a 12U satellite constraints the dimensions of the origami structure in order to fit in the usable part of the satellite (see Fig. 1). A summary of the constraints can be found in Table 2.

Table 2 Origami demonstrator constraints.

Parameter	Constraint	Description
Radius	<= 50 mm	Base inscribed circumference in order to fit in the CubeSat
Folded height	<150	For fitting in a 200 mm space within the Cubesat
Pattern	Kresling	Due to its bi-stable behavior, high inner volume, low weight and deployment response

Once these constraints are defined it is required to determine states of the origami structure, in order to improve the reader comprehension. Kresling pattern can be described in **three different states**. Here, they are described as:

- **Flat configuration.** Based on the flat pattern, which is a 2D geometry.
- **Deployed or unpacked configuration.** This refers to the 3D mounted geometry.
- **Stowed or completely folded configuration.** Refers to the state when the deployed structure is compressed in the stowed position.

Once the constraints and origami states have been defined, the problem shall be defined by its geometry, the folding processes defined, the material implemented and the optimization procedure. With all those ingredients, simulation parameters can be defined and workflow planned. Whole study, involving folding behavior has been studied under Python scripting and Abaqus FEM solver.

B. Origami geometry

Kresling pattern closure has been defined as a geometric problem to be solved [15]. Due to the bases of the geometry, this pattern is defined by triangles located around a circumference making up a cylinder-shaped geometry.

Then, the pattern could be defined by it number of sides n, the radius of the cylinder R and the height of the flat pattern h_2. According to Hunt [15], in order to form the 3D geometry, the pattern should accomplish the following equations (see Fig. 3).

$$a \cdot h_2 = d\left(\frac{d}{\tan(\varphi/2)} + \sqrt{a^2 + d^2}\right) \tag{1}$$

where a is given by the cylinder constraints (see Fig. 4) as

$$a = 2R \cdot \sin(\varphi/2) \tag{2}$$

Folding the flat pattern represented in Fig. 3 it will make up the 3D geometry shown in Fig. 4. The geometry obtained is a cylinder shape one, with the sides imposed by the flat pattern configuration.

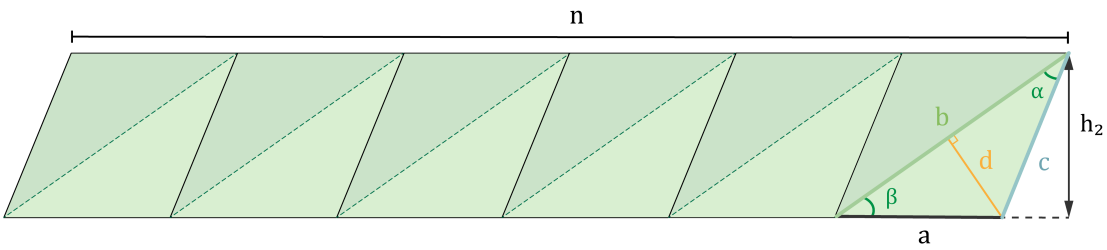

Fig. 3 Flat pattern parameters.

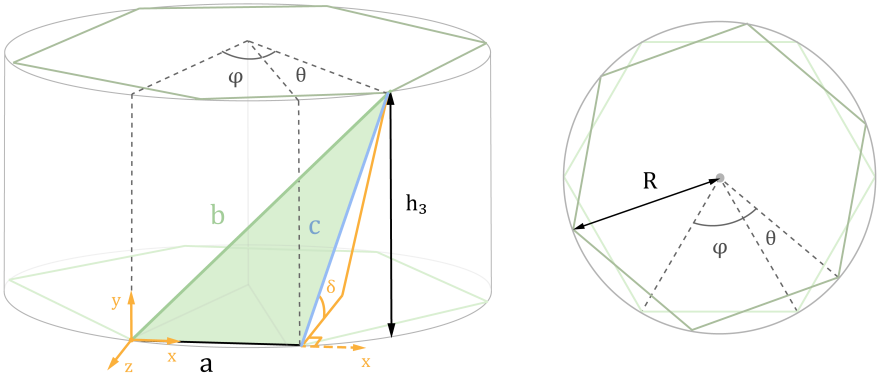

Fig. 4 3D representation.

As it is described by Berre et al. [16], the folding performance has a bi-stable response by accomplishing

$$G(h_3, \mu) = \arcsin\left(\frac{\sqrt{b^2 - h_3^2}}{2R}\right) - \arcsin\left(\frac{\sqrt{c^2 - h_3^2}}{2R}\right) - \frac{\pi}{n} = 0 \tag{3}$$

where $\mu = (b, c, n, R)$. Therefore, the design heights could be h_{3_1} and h_{3_2} defined as:

$$G(h_{3_1}, \mu) = 0 \tag{4}$$

$$G(h_{3_2}, \mu) = 0 \tag{5}$$

Being the h_{3_1} the one referred to the flat folded shape and the h_{3_2} to the one deployed. It can be easily understood in Fig. 5.

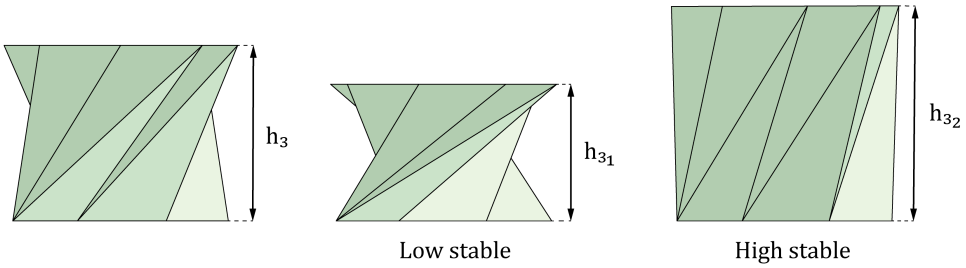

Fig. 5 Height of design according to the bi-stable behaviour. (Adapted from [16])

In order to obtain the design, the height used will be the second one, in order to regarding the real thickness and the behavior of the material used. Thus, with the dimensions of the flat pattern and the height of the 3D ori, the δ angle can be obtained. This angle is the one between the horizontal plane and the triangle of Fig. 4, *i.e.*, the angle around the x axis to reach the h_3 desired height.

C. Materials

One of the most critical problems of origami space structures is the trade-off between the stiffness and bendable properties of the pattern. A solution of compromise can be the use of two different materials, with a bendable and a stiff one.

As first approach, composite materials were considered, however for prototyping printable materials became a better solution. Most common material used with a 3D printer is the PLA (Polylactic Acid). This material shows a large rigidity when it is printed with a thickness bigger than the filament, making it difficult to fold. Therefore, it seems suitable for stiff structures but not for bendable ones. However, there are flexible printable such as the TPU (Thermoplastic Polyurethane). One of the main characteristics of this material is the capability of being one of the most versatile engineering thermoplastics materials with elastomeric properties [17].

In this case, the proposed technique is to print PLA in the regions where the stiffness is required and TPU in the crease regions. Thus, the flexibility and rigidity of the whole pattern increase. This **basic material proposal** is represented in Fig. 6.

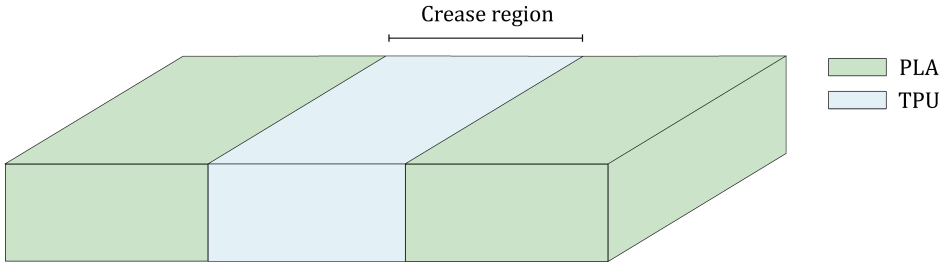

Fig. 6 Basic material proposal for printable material implementation.

Material selection is based on easier manufacturing process of printable materials. In order to print the pattern automatically, it is required a 3D printer with dual extruder. Details of prototyping are not included in the current body of work but can be consulted in the Sachithanandan study [10].

In order to define the material for the simulation as well as check its behavior, it is required to introduce the material properties. Therefore, they are summarized in Table 3.

Table 3 Material properties for rigid (PLA) and flexible (TPU) materials. [18]

	PLA (Polyactic Acid)	**TPU (Thermoplastic Polyurethane)**
Tensile modulus [MPa]	2346.5	26
Tensile strength [MPa]	49.5	8.6
Poisson module [-]	0.35	0.45
Density [g/cm3]	1.24	1.22

They are located in the main surface of the triangles and in the creases, respectively. In the Fig. 7, it is illustrated both materials. There, the rigid material (PLA) is represented with green and the flexible (TPU) with dark blue.

Thus, dual material implementation in the patter turns into the representation in Fig. 8, when the pattern is folded.

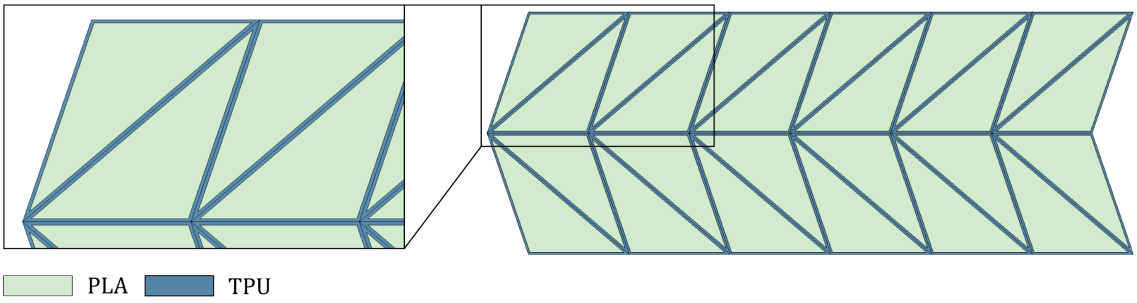

Fig. 7 Flat pattern view and material assignment.

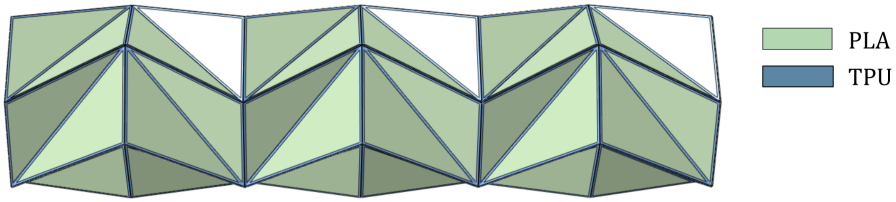

Fig. 8 Material assignment in 3D model.

Nevertheless, in order to replicate as accurate as possible the real prototype made, another material disposition was proposed. Layering was implemented for getting a joint region between both materials and for a better distribution of highest stresses. This **material layering proposal** is illustrated in Fig. 9.

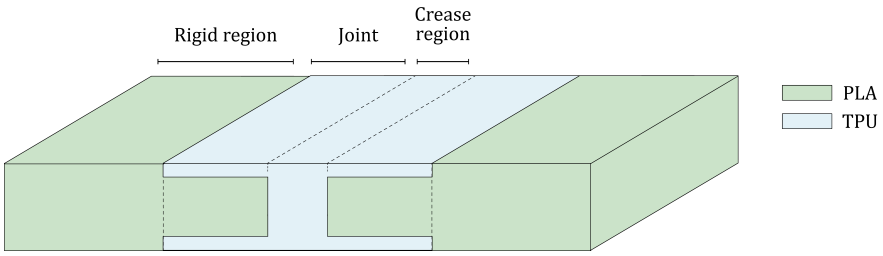

Fig. 9 Layering material proposal for printable material implementation.

This layering near the crease region is made internally and the new representation of the pattern looks like the one in Fig. 10. There it can be seen a bigger region of TPU near the crease, due to the outer layer. New material disposition can be compared with the preliminary model shown in Fig. 7.

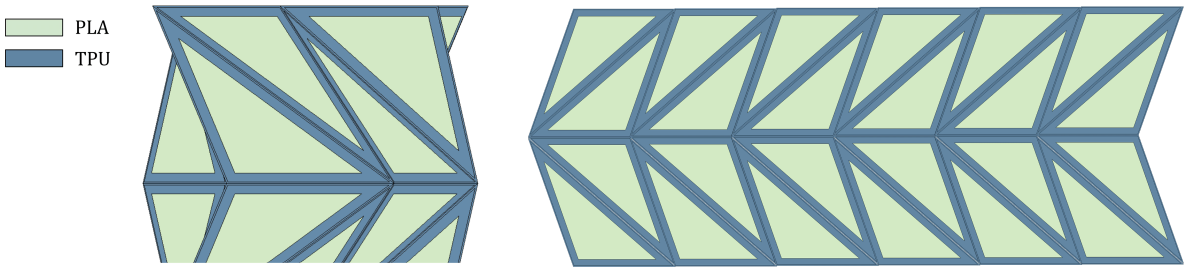

Fig. 10 Layering material proposal 3D and 2D representation.

D. Folding definition

Simulations implemented involves the movements of folding and deploying 3D ori pattern. Thus the movement is divided into two different process (folding and inflation), starting from the second stable state which is the initial state of the origami structure.

Therefore, the **folding process** is clearly illustrated in the Fig. 11. As can be seen, the movement occurs just in the vertical axis and because of the pattern properties it folds twisting. The final configuration is the folded state.

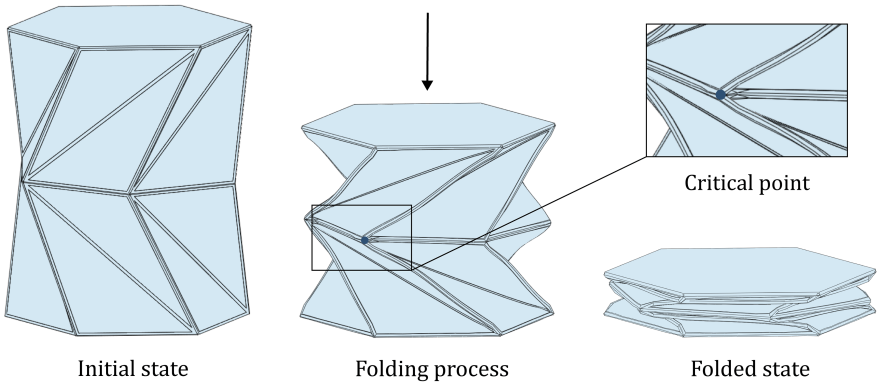

Fig. 11 Folding process.

Analysis in this study has been based on folding process due to maximum loads states. As it has be seen during the whole analysis, folding involves the maximum stress values compared with the final inflation process. Therefore, and regarding the launch loads meanwhile the pattern is folded, folding has been considered as critical structure state.

This study has been made analyzing the expected critical point of the structure, the one where eight of the triangles are in contact. Mentioned node is represented in Fig. 11, and all the results presented are related to it.

E. Boundary conditions

Under the expected behaviour during folding process, origami shall be well constrained. Boundary conditions applied can be divided into two types: constraints and loads. Corresponding the denomination used with the one implemented in Abaqus.

Constraints are used in order to fix the movement between parts and to tie them previously assembled. Therefore, two types of interactions have been used: tie and coupling. Being the ties the ones required to assemble all the triangles and the coupling the one described as follows.

- **Coupling.** Surface-based coupling constraint couples the motion of a collection of nodes on a surface to the motion of a reference node [19]. Two regions of coupling are defined in the current model.
  Firstly, as the triangle part is defined by two different materials, the flexible one shall be constrained in order to reach a feasible behaviour. Both top and bottom regions of TPU are fixed to the PLA region as seen in Fig. 12. Then, the control points are referred to the PLA vertices and the surface to the closed-polygon edges of the flexible material.

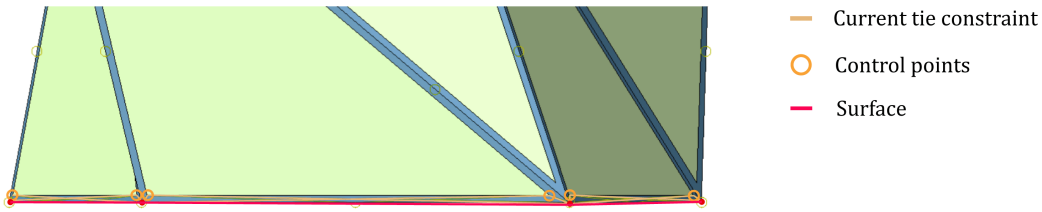

Fig. 12 Coupling constraint for top and bottom flexible material.

On the other hand, three types of loads are defined. Where load cases are defined as sets of loads and boundary conditions used to define a particular loading condition. They are described as follows.

- **Pinned.** Boundary condition applied in the bottom sides-surface in order to pinned it. Thus, translation is equal to zero in the three axes. An orange cone is illustrated in Fig. 13 for each constrained direction. This BC is **propagated in both processes**, folding and deployment.

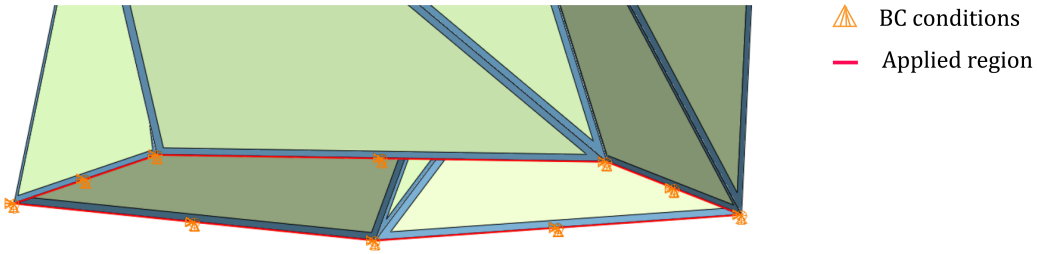

Fig. 13 Pinned boundary condition.

- **Displacement.** First folding process is defined with displacement boundary condition in order to keep the final state controlled. Thus, it is referred to the top surface defined by the top plate.

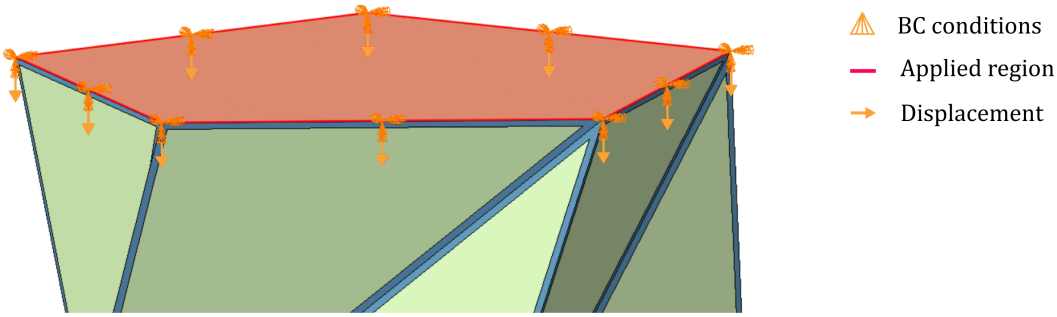

Fig. 14 Displacement boundary condition.

- **Force.** Another implemented method was a concentrated force in a reference point in the middle of the top plate. This point is pinned to all the nodes refered to the plate in order to applied a uniform force on the surface. Applied method can be seen in Fig. 15.

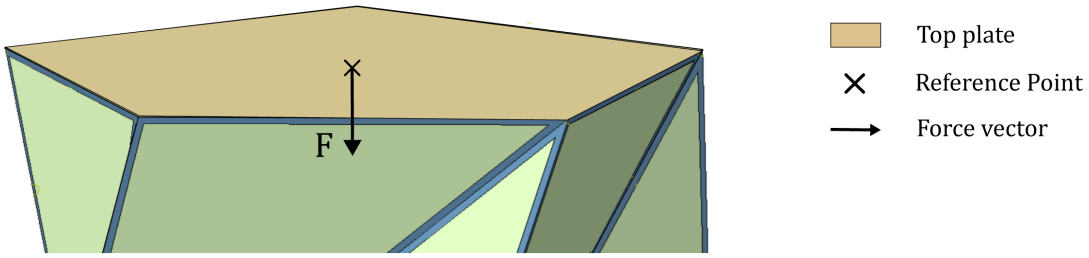

Fig. 15 Force application scheme.

This force vector is pointing due to origami base for achieving the expected folding behavior. Amplitude imposed in this force is a smooth step for a better adaptation of the model.

F. Meshing

As structural model shall be validated before assuming the results obtained, the mesh shall be independent. Experimentally, it has been discovered that the four sides Kresling pattern is the worst case for folding. This means that the ease of folding improves with the number of sides. Therefore, square-like shape is considered out of the bounds of this study and bigger number of sides is constrained due to manufacturing process.

Mesh analysis has being based on the number of elements in a side for each triangle, being this its minor value. When the element size is small enough to produce at least two rows of elements in the flexible material (see blue triangle in Fig. 16).

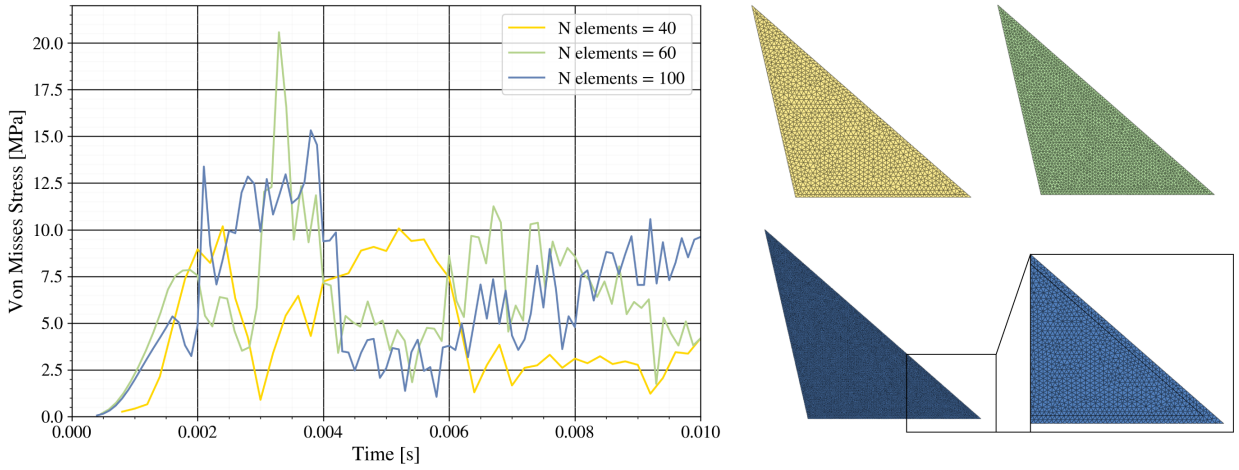

Fig. 16 Von Mises evolution for different mesh sizes (n = 5). From bigger size (40 elements per side) at upper left, to smaller size (100 elements per side below).

By narrowing the mesh elements, an almost continuous result was gotten with 130 elements per side and 6 rows in the TPU region. As can be seen in the following figure, a previous step was made by increasing the number of rows with 100 elements, but the elements were too distorted.

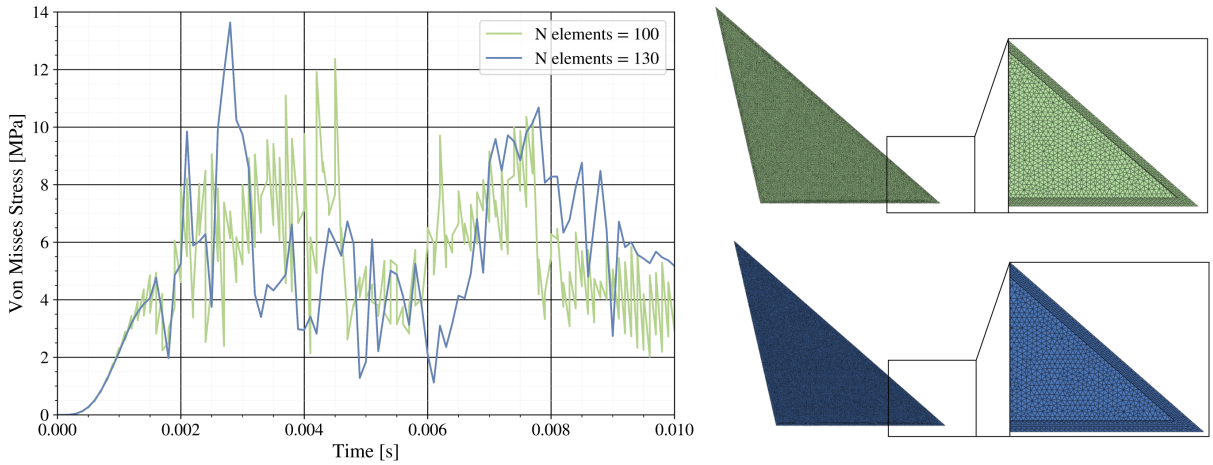

Fig. 17 Von Mises evolution for different mesh sizes (n = 5), with 6 mesh elements rows in flexible material region. From bigger size (100 elements per side) above, to smaller size (130 elements per side below).

Simulations shows that the mesh called for a distribution on the rigid region (internal one) and a smaller number of elements for reducing the simulating time.

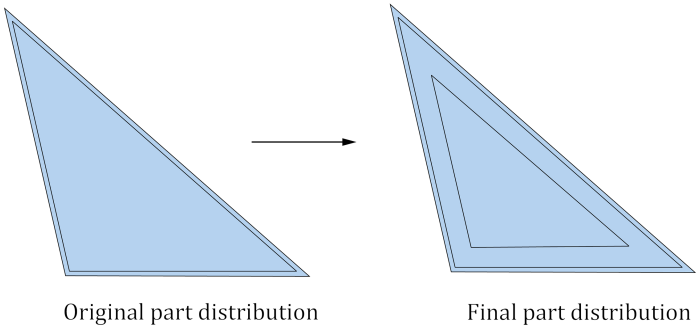

Fig. 18 Final sketch implemented for the mesh distribution.

Thus, the mesh can be based on larger elements in the inner triangle and making elements smaller towards the corners. Finally, two feasible distributions were achieved by changing the distribution and the size of the elements per edge. Fig. 19, shows the behavior of both cases compared with the best case achieved.

These three cases can be compared in number of elements per triangle, maximum mesh size and simulating time and Von Mises stress distribution. Last one illustrated in Fig. 19 and other showed in the following table.

Table 4 Resulting mesh comparison.

	130 elements	**Version 1**	**Version 2**
Number of elements per triangle	22 657	880	745
Maximum mesh size	a/130	a/20	a/20
Simulating time	11h	1h 20min	40 min

As can be seen in Table Table 4, with similar stress evolution, the finer mesh (130 elements one) and the first version differs in almost 10 hours of simulating time. Although the time is still much bigger than the expected, it means a huge improvement in the mesh analysis. Due to optimization aim, the time should be reduced as much as possible and that is why the version 2 was chosen as the best one.

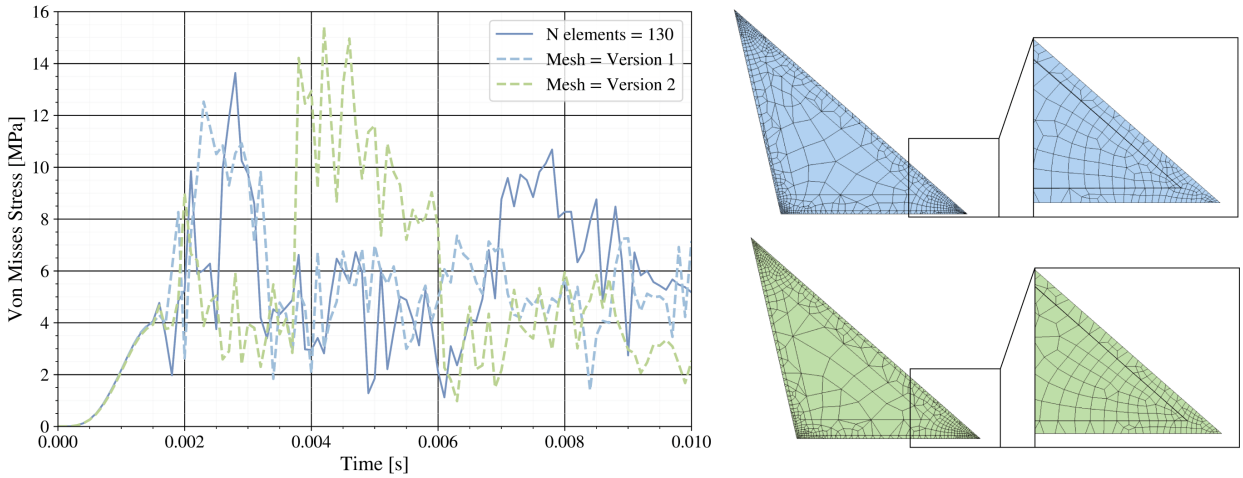

Fig. 19 Von Mises evolution for distributed meshes (n = 5). Mesh with 130 elements per side (—), distributed mesh Version 1 in blue (- -) and Version 2 in green (- -).

By reducing the simulation time in 10 hours and 20 minutes, the stress evolution follows the same path in the initial times and the maximum value still in the same magnitude order. Therefore, the mesh seems to be independent of the mesh. In order to ensure this fact, the energy balance shall first be checked.

Energy involved in the process shows the internal evolution of the structure. Balance during the simulation brings information about the accuracy of the model, as well as accuracy between both models to be compared. Firstly, the proposed distributed mesh (previously named as *Version 1*), is compared with the finer one in four different energy contributions.

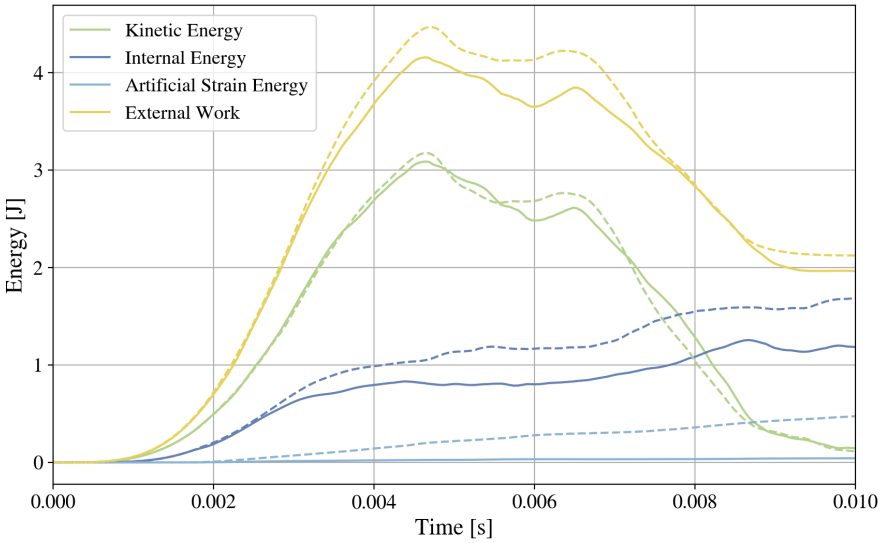

Fig. 20 Energy evolution for *130 elements* mesh (—) and *Version 2* mesh (- -).

As the folding process is based on displacement imposition, the energy evolution shows the mayor contribution comes from this external work applied (yellow lines in Fig. 20). Similar evolution is shown in the kinetic energy (green line) due to the whole displacement of the pattern. Meanwhile, internal and artificial strain energy grows with the time because the pattern folding.

Computer used for obtaining the results listed has the following processor features: Intel Core i7-9700 CPU with 8 cores at 3.00 GHz and 32.0 GB RAM.

G. Analysis outputs

Parameters to analyze are based on prototyping analysis, which means to find the best behavior of the pattern and its best replication. Therefore, outputs obtained from the analysis are divided as follows:

- **Von Mises stress.** For checking the material behavior, Von Mises stress are analyzed in order to find the maximum stress at critical points. In this case, critical point is taken as the one represented in Fig. 11.
- **Inner volume.** From the 3D formed geometry and in order to achieve a prototype for a habitat, the volume inside of the pattern is critical. Therefore, in this work two different internal volumes have been considered. First one, the **inner volume**, which is defined as the volume of cylinder that fits inside of the deployed structure. Whereas, the second volume, **outer volume**, is referred to the whole space inside of the structure. Both ones are represented in the following figure by the yellow region.

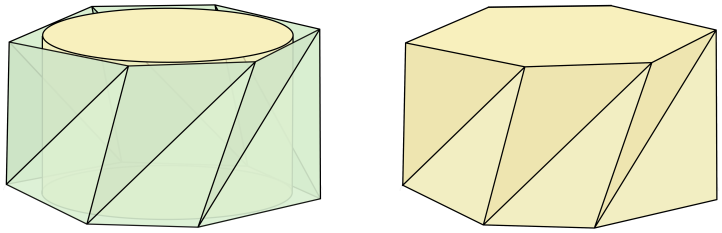

Fig. 21 Inner and outer volumes illustration.

III. Results

Because this study is focused on the structure and modeling of the origami demonstrator, the physical behavior of the pattern must be known. Then two models have being defined in order to analyze the physical response, as they are configured in Table 5.

Table 5 Models under analysis description.

Model type	Material configuration	Constraints	Loads
Basic model	Basic	Tie + Coupling	Pinned + Displacement
Advanced model	Layering	Tie	Pinned + Concentrated Force

Kresling pattern movement is known for being independent by each ring, being able to fold and deploy them one by one. [8] Then, movement obtained in the numerical model shall achieve this behavior in order to ensuring the veracity of the whole model. It can be described by a sequence of movements: twist and bending as it is shown in Fig. 22. Both of them are sequentially occurring as:

- **First twist.** First ring starts to fold twisting favoring the turn indicated by the fold direction.
- **First bending.** This twisted ring starts bending as the twisting is getting completed.
- **Second twist.** When the first ring is completely folded, the second one repeat the first twist in the reverse direction.
- **Second bending.** By helping the twist, the second ring gets consequently folded.

This sequence of movements can be seen in the following diagram, where two rings of a greater origami pattern folds one by one.

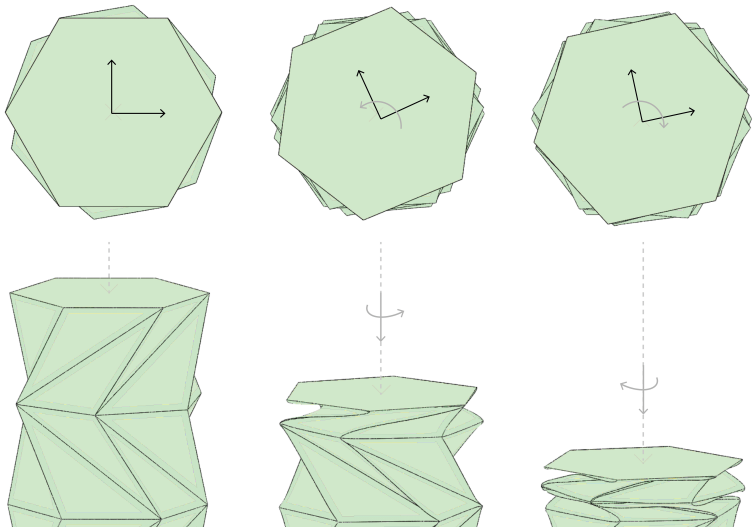

Fig. 22 Kresling physical behavior.

Regarding this motion as the base motion of the system, a study can be carried out on the results obtained for both models under study: under imposition of displacements for **Basic model** and constant force for **Advanced model**.

A. Basic model

For obtaining preliminary conclusions from this first model, several simulations were done by modifying its parameter values (n, N and R). Here, controlling by displacement the movement is imposed on the top plate, constraining it to an almost linear one. In this case, the amplitude considered was an smooth step in order to make easier the folding process at the beginning of the simulation.

- **Dual material distribution.** Prototyping and manufacturing analysis made by Sachithanandan [10] shows the requirement of a join region for both materials. This joining is made with a 3 mm offset around the crease for assuring the unity of the cylinder (see Fig. 23). Printing a thin TPU layer over the stiff PLA, allows to fix them in order to ensure a composite material made by theses two ones.

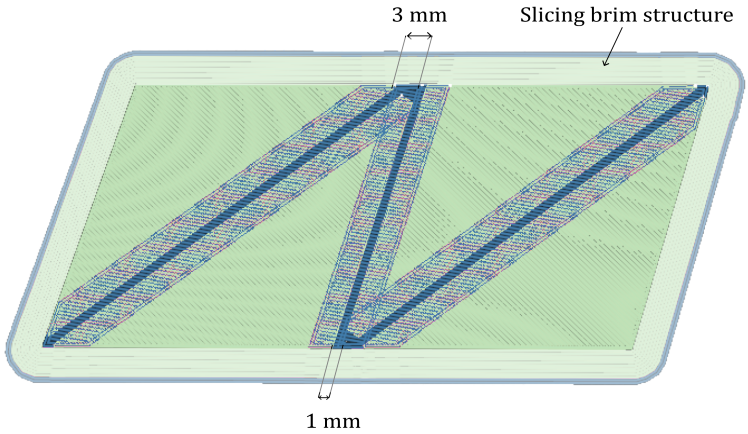

Fig. 23 3D print overlap near crease region. [Adapted from [10]]

- **Non physical behavior.** By imposing the displacement of the origami top plate, whole model movement is imposed and its evolution is a smooth step function. Although Kresling folding evolution is not a linear movement it is imposed from a higher level. Thus, results obtained from this model are not as physical as it would be desired, being required to characterize Kresling natural movement.

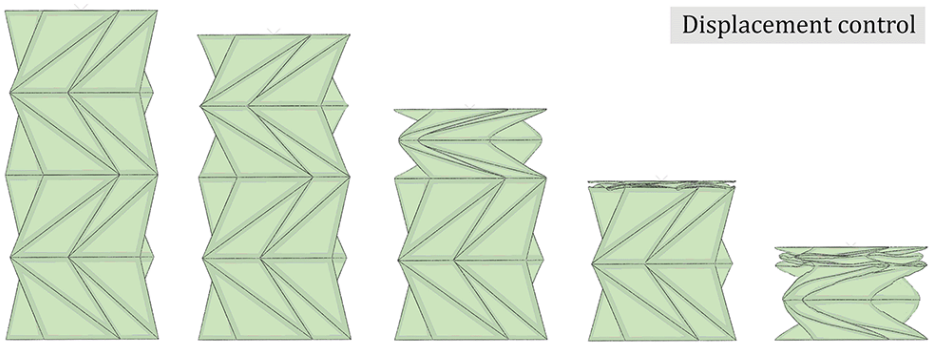

Fig. 24 Physical behavior during folding for displacement control.

- **Over-constrained bounds** As the model is defined by an unique part assembled, a coupling constraint is used for restrict the movement on the TPU region in the base. Nevertheless, coupling here is over-constraining the Kresling base.

B. Advanced model

Based on conclusions obtained from *Basic model* some features have been modified in order to improve the model behavior and its accuracy. Following the aim of characterizing the prototype model, improvements listed as follows has been established.

- **Layering configuration.**Nevertheless, apart from being a manufacturing feature, new material distribution provides as well a structural improvement. As can be seen in Fig. 25 the addition of TPU layer near the crease produce a better distribution of the stress among this region.

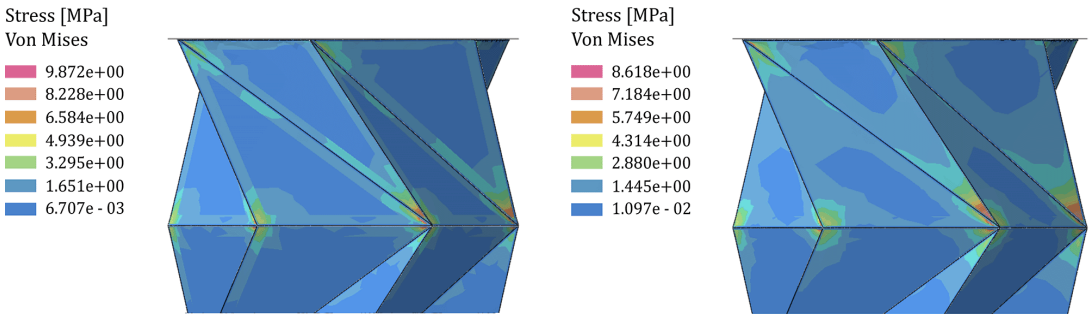

Fig. 25 Von Mises Stress distribution. New material (Left) and old material (Right) configurations.

- **Constraints at base.** As the coupling on the base results as an over-constrained region, skip this interaction should improve the model behavior. Therefore a new part was created without flexible material on the base. Resulting on a cylindrical structure made of triangles of stiff material just joined by a flexible one at each crease.

- **Concentrated force control.** As the movement is not imposed and the origami is folded just by force application, displacement remains as a free parameter of the system and a non-linear behavior appears. Then the folding movement has been analyzed for different number of rings, studying the evolution depending on this N parameter.

Results obtained for this case has been got by imposing a constant force value, in order to find a common value for folding all the rings.
As it was obtained for displacement control, physical behavior has been as well studied. As it is shown in Fig. 26, for this case, each rings folds independently and in an orderly manner. Behavior which corresponds to what should be expected in Kresling displacement [8].

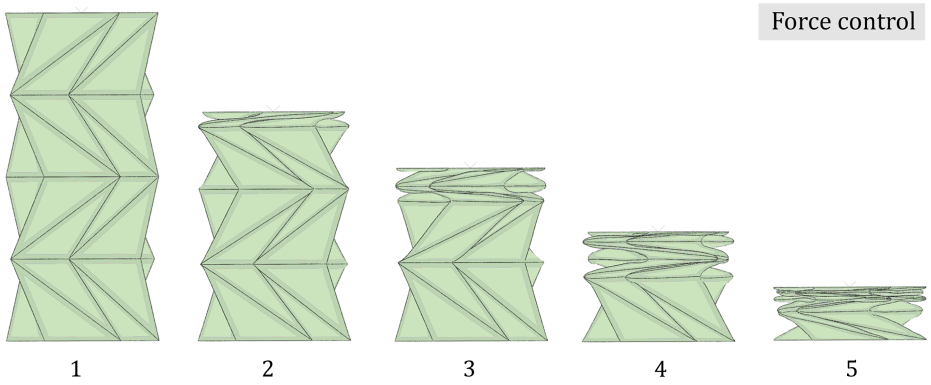

Fig. 26 Physical behavior during folding for force control.

These five displacement states are related to the points represented in Fig. 27. Where it is illustrated the External Work during the whole folding, which is inversely proportional to the resulted displacement. Then, it is seen the non-linear behavior of the Kresling pattern when force is imposed (instead of displacement) and the folding evolution of each ring can be better understood.

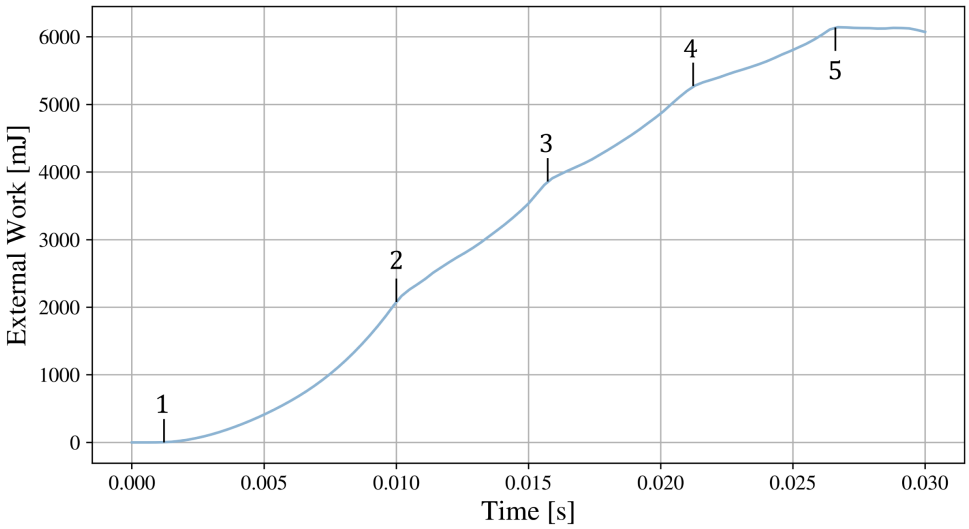

Fig. 27 Physical behavior during folding for force control.

For a generalized view of the problem, the following figure (Fig. 28) shows the evolution of the External Work for each value of N, from 1 to 6, in front of the time. Then, folding time for each ring can be almost characterized or at least better clarified for the reader.

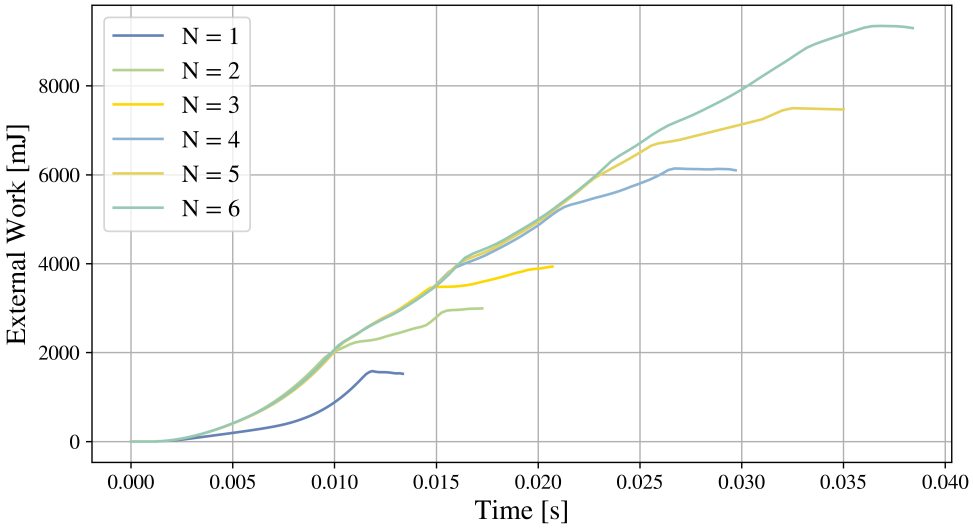

Fig. 28 External work [mJ] in front of simulation time [s].

For each value of N, non linear behavior is shown, and folding evolution is clearly seen for each ring. Then, some conclusions can be obtained from this External Work evolution.

- Each ring gets completely folded when it reach the slope change. Thus, it can be seen the number of rings on this evolution folding in similar time steps.
- For the case in which $N = 1$ the evolution is different from the other cases as this folding process is one ring constrained both on top and base. Thus, the last ring folds faster for the six cases than the time it takes for folding with higher values of N.
- For other cases ($N > 1$), the curve follows the same path at least until the first ring is folded, *i.e.* before 0.01 seconds. Then, the evolution changes depending on the total number of rings due to the twist and initial folding behavior for Kresling pattern.

This force control response seems to be more physically meaningfull than displacement control stated on the basic model. As it is reported such behavior on paper models studied by Kidambi and Wang [20].

C. Optimization

Following the LHS theory, the resulting samples are defined inside of a quadrilateral area,*i.e.*., the region is defined as linear. Nevertheless, by try and error, a correlation was obtained calculating the second bi-stable solution: not all geometries accomplished this condition. Moreover, the smaller number of sides the harder it gets the folding process, being smoother from almost 6 sides. However, in the manufacturing process developed by Sachithanandan [10], the larger the number of sides the harder it takes the initial folding of the pattern. Therefore, this analysis was focused on the region between 6 and 12 sides.

From above constraints, minimum and maximum values of flat height have been calculated for n (from 4 to 20) and the fixed value of R (50mm). Fig. 29 shows both mentioned limits and the region inside them, which involves the solution region.

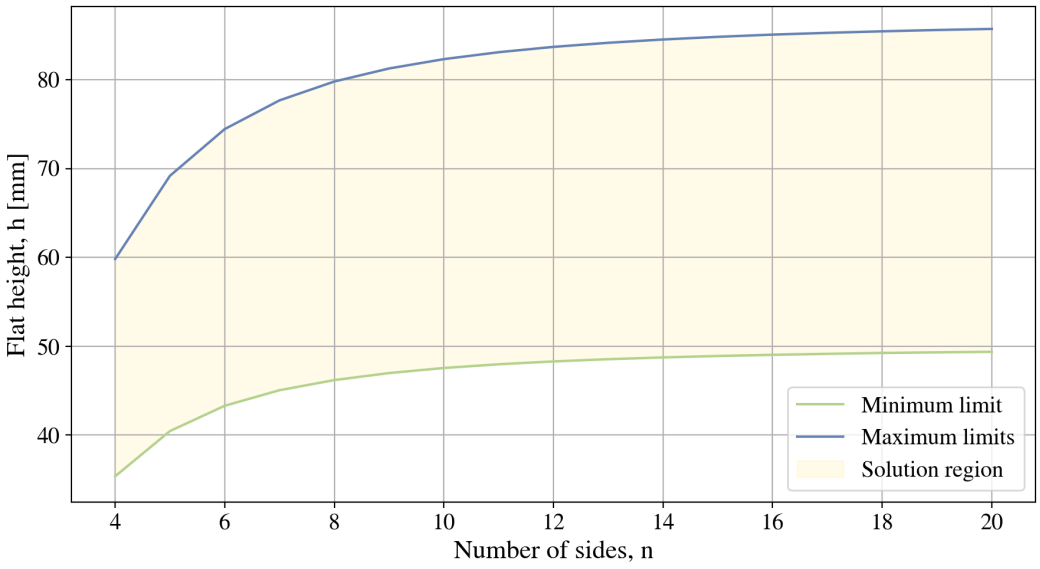

Fig. 29 Maximum and minimum h values limits for feasible Kresling geometries.

Applying LHS using the Python Library *SMT*, sampled data can be obtained inside the region between the minimum and the maximum limits. As result, feasible configurations of the pattern are represented in Fig. 30 within the *solution region*.

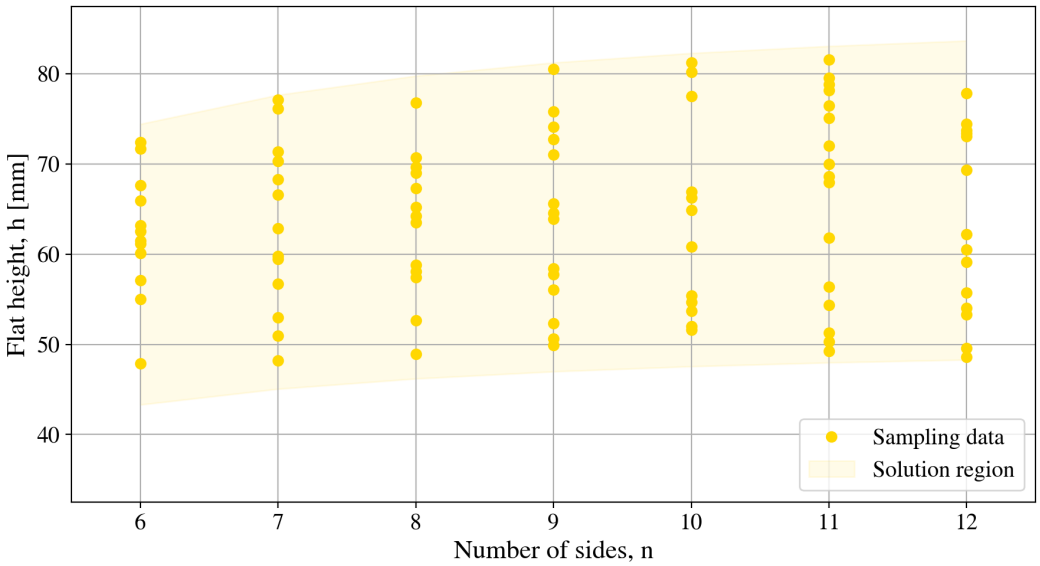

Fig. 30 Corrected sampling results.

From the seven cases of analysis mentioned (N value from 6 to 12), optimum values were obtained thanks to Dakota solver implementing MOGA. By **minimizing maximum Von Mises stress** and **maximizing inner volume**, each number of sides has an involved optimum case. Thus, obtained results are grouped together in Fig. 31.

Optimized results were obtained with following GA parameters:

- **Population size:** 800
- **Number of generations:** 100

Where dashed lines are not part of the surrogate model, is the polynomial approximation (according to the surrogate polynomial degree) illustrated for a better comprehension of the reader.

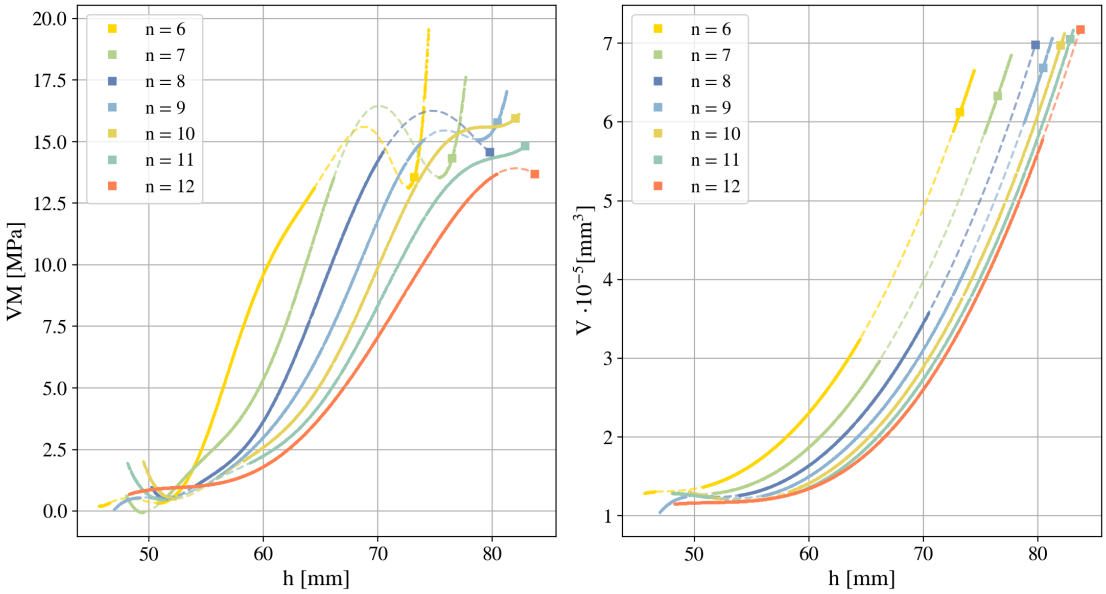

Fig. 31 Optimum results evolution for the cases under study. Von Mises stress (left) and Inner volume (right).

Therefore, in maximum stress distribution, by increasing the flat height h the results made an "S" shape behavior, meanwhile in volume results it is half of an opened "U" response. However, by zooming in the regions near optimum solution, a valley in maximum values of Von Mises stress that shows the interest region. Obtaining, nonetheless, an almost linear evolution in the case of volume.

As the solution points there are limited by the stress, optimum behavior is in most cases, in the point where the stress slope clearly changes. Which can be described in an optimization context, the point of interest.

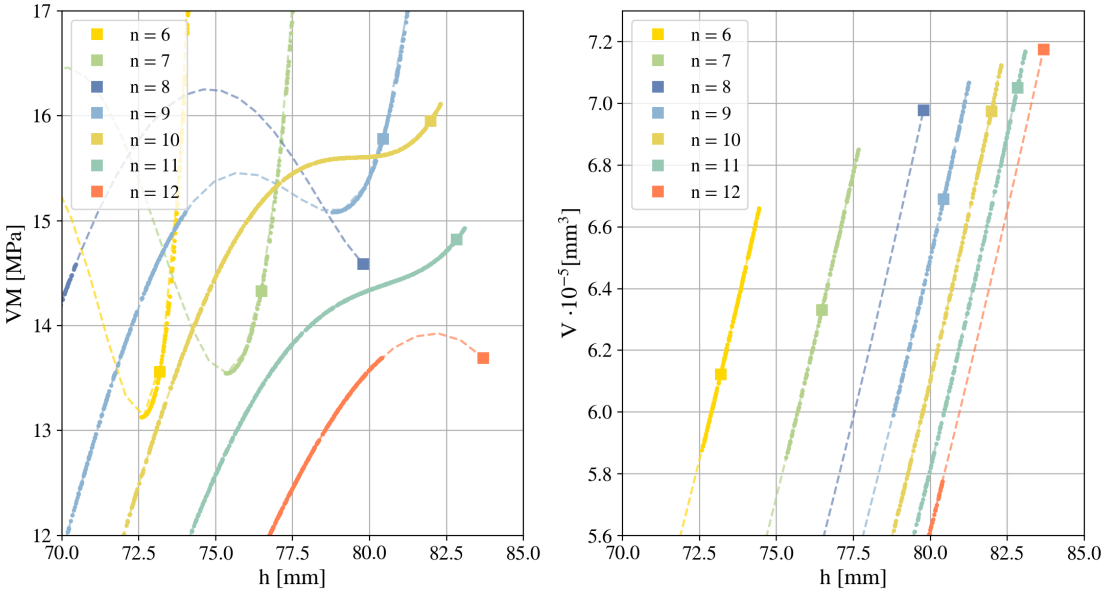

Fig. 32 Zoom of optimum results evolution for the cases under study.

Overall, by the depicted Von Mises stress in front of Volume, results shows a non-dependency response due to eight sides results. Nevertheless, this value was checked with the surrogate results and, as can be seen in the figure, optimum case is much near to a real solution. Thus, this result shall be considered as well as feasible one. From a Pareto Front it would be expected a curve with a tendency for results, however obtained ones shows a non-clear correlation between stress and internal volume. Because of that, results need to be validated and checked independently.

IV. Conclusion

This study investigates origami-inspired deployable structures as a viable solution to the space industry's demand for pressurized, large structures. The goal of this project has been to design and optimize an origami-inspired deployable structure for use as a technology demonstrator within a 12U CubeSat.

With some selections regarding the specific origami pattern, deployment mechanism, and material considerations, parameterized models made by Python scripting were implemented. The generated code in the presented work includes the creation of variable origami patterns, the modeling of printable materials, and the meshing for numerical analysis. The entire analysis process was completed, beginning with mathematical implementation for geometry definition and ending with optimization analysis.

Preliminary analysis was made to insure the accuracy of the parameterized model. Although the parameterization was achieved for the three parameters considered (R, N and n), the model called for an improvement in order to better represent the prototyped model. Therefore, an advanced model was developed including an advanced material layering model and neglecting coupling constraints.

In parallel, two approaches were studied for understanding the Kresling pattern behavior: displacement and force control. The first model, described as the basic model in this document, is based on displacement and shows almost linear behavior, which does not correspond with the observed behavior. The second model, described as the advanced model in this document, achieves the expected response by folding one ring at a time, in an orderly manner, and independently. Additionally, each ring folding exhibits a unique slope evolution, or non-linear behavior, and each change in slope indicates whether or not a ring has successfully folded.

The optimization process did not yield a single solution in which a configuration pattern performs the best with all the criteria chosen. Nonetheless, a "S"-shaped result was obtained for stress evolution for height values as a function of the number of sides and a "U"-shaped result for volume evolution. These results were obtained with the *Version 1* mesh, which was not the best one at continuous results but the best in a trade-off performance. Therefore, an analysis with a finer mesh may be required in order to verify the obtained behavior.

This work is part of the first steps in characterizing an origami-inspired deployable structure part of a Cubesat demonstrator. The project will hopefully lay the groundwork for future advances in origami-inspired design within the context of space-deployable structures.

Acknowledgments

The authors would like to thank Dr. Javier Paz Mendez and Dr. Marta María Moure Cuadrado for their help and insight throughout this research, and Joshika Sachithanandan MSc. for her contributions, thoughts and help during the development of the origami numerical models.

References

[1] Meloni, M., Cai, J., Zhang, Q., Sang-Hoon Lee, D., Li, M., Ma, R., Parashkevov, T. E., and Feng, J., "Engineering origami: A comprehensive review of recent applications, design methods, and tools," *Advanced Science*, Vol. 8, No. 13, 2021, p. 2000636.

[2] Haraszti, A., and Arya, M., "Origami-Inspired Closeouts for Starshade Inner Disk Optical Shields," *International Design Engineering Technical Conferences and Computers and Information in Engineering Conference*, Vol. 86281, American Society of Mechanical Engineers, 2022, p. V007T07A065.

[3] Valle, G. D., Litteken, D., and Jones, T. C., "Review of habitable softgoods inflatable design, analysis, testing, and potential space applications," *AIAA Scitech 2019 Forum*, 2019, p. 1018.

[4] Yang, M., Defillion, J., Scarpa, F., and Schenk, M., "Volume Optimisation of Multi-stable Origami Bellows for Deployable Space Habitats," *Acta Mechanica Solida Sinica*, 2023, pp. 1–17.

[5] Spencer, D. A., Betts, B., Bellardo, J. M., Diaz, A., Plante, B., and Mansell, J. R., "The LightSail 2 solar sailing technology demonstration," *Advances in Space Research*, Vol. 67, No. 9, 2021, pp. 2878–2889.

[6] Cai, J., Deng, X., Feng, J., and Zhou, Y., "Geometric design and mechanical behavior of a deployable cylinder with Miura origami," *Smart Materials and Structures*, Vol. 24, No. 12, 2015, p. 125031.

[7] Suh, J., Kim, T., and Han, J.-H., "New Approach to Folding a Thin-Walled Yoshimura Patterned Cylinder," *Journal of Spacecraft and Rockets*, 2020. https://doi.org/10.2514/1.A34784.

[8] Jianguo, C., Xiaowei, D., Ya, Z., Jian, F., and Yongming, T., "Bistable behavior of the cylindrical origami structure with Kresling pattern," *Journal of Mechanical Design*, Vol. 137, No. 6, 2015, p. 061406.

[9] Uriol, I., and Solano-López, P., "Preliminary Study of An Origami-inspired Deployable Structure for a Small-Scale Demonstrator," *73rd International Astronautical Congress (IAC)*, Paris, France, 2022, pp. IAC–22–C2.IP.

[10] Sachithanandan, J., Uriol, I., and Solano-López, P., "Preliminary Design of a CubeSat Demonstrator for an Origami-inspired Deployable Structure," *74th International Astronautical Congress (IAC)*, Baku, Azerbaijan, 2023.

[11] Yang, K., Xu, S., Zhou, S., and Xie, Y. M., "Multi-objective optimization of multi-cell tubes with origami patterns for energy absorption," *Thin-Walled Structures*, Vol. 123, 2018, pp. 100–113. https://doi.org/https://doi.org/10.1016/j.tws.2017.11.005, [Online]. Available: https://www.sciencedirect.com/science/article/pii/S0263823117309643.

[12] Sarabia, L., and Ortiz, M., "1.12 - Response Surface Methodology," *Comprehensive Chemometrics*, edited by S. D. Brown, R. Tauler, and B. Walczak, Elsevier, Oxford, 2009, pp. 345–390. https://doi.org/https://doi.org/10.1016/B978-044452701-1.00083-1, [Online]. Available: https://www.sciencedirect.com/science/article/pii/B9780444527011000831.

[13] Paz Méndez, J., "Crashworthiness analysis and design optimization of hybrid energy absorption devices: application to aircraft structures," Ph.D. thesis, Universidade da Coruña, 2018. Available: http://hdl.handle.net/2183/21137.

[14] Mckay, M. D., Beckman, R. J., and Conover, W. J., "A Comparison of Three Methods for Selecting Values of Input Variables in the Analysis of Output from a Computer Code," 2023. https://doi.org/https://doi.org/10.2307/1268522, [Online]. Available: http://www.jstor.org/stable/1271432.

[15] Hunt, G. W., and Ario, I., "Twist buckling and the foldable cylinder: an exercise in origami," *International Journal of Non-Linear Mechanics*, Vol. 40, No. 6, 2005, pp. 833–843. https://doi.org/https://doi.org/10.1016/j.ijnonlinmec.2004.08.011.

[16] Berre, J., Geiskopf, F., Rubbert, L., and Renaud, P., "Toward the Design of Kresling Tower Origami As a Compliant Building Block," *Journal of Mechanisms and Robotics*, Vol. 14, 2021, pp. 1–12. https://doi.org/10.1115/1.4053378, [Online]. Available: https://www.researchgate.net/publication/357311947_Towards_the_design_of_Kresling_tower_origami_as_a_compliant_building_block.

[17] Brancewicz-Steinmetz, E., Sawicki, J., and Byczkowska, P., "The Influence of 3D Printing Parameters on Adhesion between Polylactic Acid (PLA) and Thermoplastic Polyurethane (TPU)," *Materials*, Vol. 14, 2021, p. 6464. https://doi.org/10.3390/ma14216464.

[18] Xometry Europe GmbH, "3D Printing Materials," , 2023. [Online]. Available: https://xometry.eu/en/ms/3d-printing/.

[19] ABAQUS, *Online Documentation: Version 6.6-1*, ABAQUS, Inc., 2014.

[20] Kidambi, N., and Wang, K. W., "Dynamics of Kresling origami deployment," *Physical Review E*, Vol. 101, No. 6, 2020. https://doi.org/10.1103/physreve.101.063003, = https://doi.org/10.1103%2Fphysreve.101.063003.